

Pressure-volume-temperature equation of state of MgSiO₃ perovskite from molecular dynamics and constraints on lower mantle composition

Frederic C. Marton, Joel Ita,¹ and Ronald E. Cohen

Geophysical Laboratory and Center for High Pressure Research,
Carnegie Institution of Washington, Washington, D. C.

Abstract

The composition of the lower mantle can be investigated by examining densities and seismic velocities of compositional models as functions of depth. In order to do this it is necessary to know the volumes and thermoelastic properties of the compositional constituents under lower mantle conditions. We determined the thermal equation of state (EOS) of MgSiO₃ perovskite using the nonempirical variational induced breathing (VIB) interatomic potential with molecular dynamics simulations at pressures and temperatures of the lower mantle. We fit our pressure-volume-temperature results to a thermal EOS of the form $P(V, T) = P_0(V, T_0) + \Delta P_{\text{th}}(T)$, where $T_0 = 300$ K and P_0 is the isothermal Universal EOS. The thermal pressure ΔP_{th} can be represented by a linear relationship $\Delta P_{\text{th}} = a + bT$. We find $V_0 = 165.40 \text{ \AA}^3$, $K_{T_0} = 273$ GPa, $K'_{T_0} = 3.86$, $a = -1.99$ GPa, and $b = 0.00664$ GPa K⁻¹ for pressures of 0-140 GPa and temperatures of 300-3000 K. By fixing V_0 to the experimentally determined value of 162.49 \AA^3 and calculating density and bulk sound velocity profiles along a lower mantle geotherm we find that the lower mantle cannot consist solely of (Mg,Fe)SiO₃ perovskite with X_{Mg} ranging from 0.9-1.0. Using pyrolitic compositions of 67 vol % perovskite ($X_{\text{Mg}} = 0.93$ -0.96) and 33 vol % magnesiowüstite ($X_{\text{Mg}} = 0.82$ -0.86), however, we obtained density and velocity profiles that are in excellent agreement with seismological models for a reasonable geotherm.

1. Introduction

By comparing density and seismic velocity profiles of compositional models with seismological models it is possible to investigate the composition of the Earth's lower mantle. Therefore an understanding of the high pressure, high temperature properties, and equation of state (EOS) of (Mg,Fe)SiO₃ perovskite is vital to our understanding of the lower mantle, as this mineral accounts for perhaps two thirds of the mineralogy of this region [Bina, 1998] and one third of the volume of the entire planet. Experiments have been performed up to pressures approaching those found at the base of the mantle, but direct coverage of the lower mantle geotherm has been limited to perhaps the uppermost one third (Figure 1). Experiments include resistively heated multianvil apparatus [Wang *et al.*, 1994; Kato *et al.*, 1995; Utsumi *et al.*, 1995; Funamori *et al.*, 1996], diamond anvil cells (DACs) at ambient temperature [Kudoh *et al.*, 1987; Ross and Hazen, 1990], resistively heated DACs [Mao *et al.*, 1991; Saxena *et al.*, 1999], laser heated DACs [Knittle and Jeanloz 1987; Fiquet *et al.*, 1998, 2000], and shock wave experiments [Duffy and Ahrens, 1993; Akins and Ahrens, 1999].

Theoretical methods, such as those used here, permit the investigation of thermodynamic and thermoelastic properties of minerals at high pressures and temperatures. Previous theoretical work on orthorhombic MgSiO₃ perovskite (Mg-pv) has been done using molecular dynamics (MD) using the semi-empirical potential of Matsui [1988] at 0-1000 K and 0-10 GPa (at 300 K) [Matsui, 1988] and 300-5500 K and 0-400 GPa [Belonoshko, 1994; Belonoshko and Dubrovinsky, 1996] and combined with lattice dynamics at 500-3000 K and 0-100 GPa [Patel *et al.*, 1996]. Wolf and Bukowinski [1987] used a rigid ion modified electron gas (MEG) model at 0-800 K and 0-150 GPa, while Hemley *et al.* [1987] used a MEG model combined with shell stabilized ion charge densities at 0-2500 K and 0-200 GPa. Cohen [1987] did quasi-harmonic lattice dynamics calculations from 0-3000 K and 0-150 GPa using the potential induced breathing (PIB) model. First principles static lattice calculations ($T = 0$ K) have also been done up to pressures of 150 GPa, using plane wave pseudopotential (PWPP) MD [Wentzcovitch *et al.*, 1995] and the linearized augmented plane wave (LAPW) method [Stixrude and Cohen, 1993]. Karki *et al.* [1997] also used the PWPP method to examine the athermal elastic moduli of Mg-pv.

In addition to the equation of state the thermodynamic stability of perovskite in the lower mantle is an open question and has been studied with experimental and theoretical methods. Work by Meade *et al.* [1995], Saxena *et al.* [1996, 1998], and Dubrovinsky *et al.* [1998] indicate that perovskite will break down to oxides under lower mantle conditions. The thermodynamic analysis of Stixrude and Bukowinski [1992] and the experimental work of Serghiou *et al.* [1998], however, suggest that it will not.

We used MD simulations using the nonempirical variational induced breathing (VIB) model, similar to the model of Wolf and Bukowinski [1988], to investigate the properties and EOS of Mg-pv at pressures (0-140 GPa) and temperatures (300-3000 K) that cover the bulk of the conditions found in the lower mantle. Newton's equations of motion are solved as functions of time, and equilibrium properties are obtained as time averages over a sufficiently long interval. This accounts for all orders of anharmonicity but not for quantum lattice dynamics effects. Thus our results are more appropriate at high temperatures above the Debye temperature (1076 K [Anderson, 1998]) and are entirely suitable for the Earth's mantle. We then used our results, combining them with data for other components and phases where appropriate, to calculate density and seismic velocity profiles along a geothermal gradient for different compositional models. These profiles were then compared with profiles from a reference Earth model in order to test the compositional models' fitness for the lower mantle.

2. Method

MD simulations were performed on supercells of 540-2500 atoms of orthorhombic (*Pbnm*) Mg-pv using the nonempirical VIB potential. VIB is a Gordon-Kim type model [Gordon and Kim, 1972], where the potential is obtained by overlapping ionic charge densities which are computed using the local density approximation (LDA) [Hedin and Lundqvist, 1971]. The total energy is a sum of (1) the self-energy of each atom, (2) the long-range electrostatic energy computed using the Ewald method, and (3) the short-range interaction energy, i.e., the sum of the kinetic, short-range electrostatic, and exchange-correlation overlap energies from the LDA. Free oxygen ions are not stable and are stabilized in VIB by surrounding them with Watson spheres with charges equal in magnitude but opposite in sign to the ions, e.g., 2+ spheres for O²⁻. Interactions are obtained

for overlapping ion pairs at different distances with different Watson sphere radii for each oxygen. The interactions are fit with a 23-parameter analytical expression as functions of the interatomic distance r and $U_i = z_i/R_i$, where U_i , z_i , and R_i are the Watson sphere potential, charge, and radius for atom i . For each oxygen i , R_i is adjusted to minimize the total energy at each time step. This gives an effective many-body potential. The oxygen ions respond to changes in their environment. For example, they are compressed at high pressures relative to low pressures. Previous work on Mg-pv using the related PIB model gave an equation of state in excellent agreement with experiment [Cohen, 1987]. Also, work using VIB on MgO has shown that this model accurately predicts EOS and thermal properties [Inbar and Cohen, 1995].

Nominally charged ions give semiquantitative, but less accurate, results than desired for Mg-pv. This is due to a small degree of covalent bonding relative to ionic bonding as revealed by electronic structure calculations of cubic ($Pm3m$) Mg-pv performed using the first principles LAPW method [Cohen *et al.*, 1989]. These calculations show that while the Mg is nearly a perfectly spherical Mg^{2+} ion, there is some charge transfer from O to Si and a small covalent bond charge (involving $\ll 0.1$ electrons) between Si and O. By varying the ionic charges on Si (3.1+ to 3.55+) and O (1.70- to 1.85-) to account for the covalency, but otherwise using the same methods as before, we compared the resulting zero temperature pressure-volume data to the LAPW results of *Stixrude and Cohen* [1993]. The best agreement was found with $Si^{3.4+}$ and $O^{1.8-}$. Using these charges, the resulting potential gives excellent agreement with the octahedral rotation energetics obtained using the LAPW method [Stixrude and Cohen, 1993; Hemley and Cohen, 1996] (Figure 2).

MD runs were performed for 20 ps with a 1 fs time step using a sixth-order Gear predictor-corrector scheme [Gear, 1971] in the constant pressure-temperature ensemble using the thermostat and barostat of *Martyna et al.* [1994]. Initial atomic positions for the genesis run were the same as those for the unrotated octahedra of *Stixrude and Cohen* [1993]. Subsequent runs at higher pressures or temperatures used the positions generated by a previous run. Statistical ensembles were obtained in ~ 2000 iterations for the genesis run and in < 1000 iterations for subsequent runs.

We fitted pressure-volume-temperature (P-V-T) data obtained from the MD simulations to a thermal

EOS of the form

$$P(V, T) = P_0(V, T_0) + \Delta P_{th}(T) \quad (1)$$

with a reference temperature $T_0 = 300$ K and the thermal pressure ΔP_{th} relative to the 300 K isotherm. We analyzed our results using the third-order Birch-Murnaghan isothermal EOS [Birch, 1952]

$$P_0 = 3K_{T_0}f(1 + 2f)^{5/2}(1 - \xi f), \quad (2)$$

with the Eulerian strain variable f and the coefficient ξ given by

$$f \equiv \frac{1}{2} \left[\left(\frac{V_0}{V} \right)^{2/3} - 1 \right], \quad \xi \equiv -\frac{3}{2}(K'_{T_0} - 4), \quad (3)$$

and the Universal EOS [Vinet *et al.*, 1987]

$$P_0 = 3K_{T_0}(1-x)x^{-2} \exp \left[\frac{3}{2}(K'_{T_0} - 1)(1-x) \right], \quad (4)$$

where $x = (V/V_0)^{1/3}$, K_T is the isothermal bulk modulus, and K'_T is its pressure derivative.

ΔP_{th} is given by

$$\Delta P_{th} = \int_{T_0}^T \left(\frac{\partial P}{\partial T} \right)_V d\hat{T} = \int_{T_0}^T (\alpha K_T) d\hat{T}, \quad (5)$$

where α is the volume coefficient of thermal expansion. If αK_T is independent of T , then the thermal pressure can be represented by a linear relationship [Anderson, 1980, 1984; Anderson and Suzuki, 1983]

$$\Delta P_{th} = a + bT, \quad (6)$$

which applies to a wide range of solids at high T , including minerals, alkali metals, and noble gas solids [Anderson, 1984]. The linearity of ΔP_{th} in T starts at 300 K [Masuda and Anderson, 1995] in minerals. There should be a small anharmonic correction at high T , which results in an additional cT^2 term in (6), which is often sufficiently small so that it can be neglected [Anderson, 1984]. Indeed, including the cT^2 term did not statistically improve our fits. Likewise, our fits were not improved by including volumetric compression terms [e.g., Jackson and Rigden, 1996].

Once the P-V-T data were fit, other parameters, such as α ,

$$\alpha = \left(\frac{\partial \ln V}{\partial T} \right)_P, \quad (7)$$

its volume dependence, the Anderson-Grüneisen parameter,

$$\delta_T = \left(\frac{\partial \ln \alpha}{\partial \ln V} \right)_T, \quad (8)$$

the Grüneisen parameter,

$$\gamma = \frac{\alpha K_T V}{C_V}, \quad (9)$$

and its volume dependence,

$$q = \left(\frac{\partial \ln \gamma}{\partial \ln V} \right)_T, \quad (10)$$

were obtained by numerical differentiation. C_P was found by calculating enthalpy ($U + PV$) at each MD run point and differentiating with respect to T . Using the relation $C_P = C_V(1 + \gamma\alpha T)$, equation (9) can be rewritten as

$$\gamma = \left(\frac{C_P}{\alpha K_T V} - T\alpha \right)^{-1}. \quad (11)$$

3. Results

MD calculations were performed at 46 pressure-temperature (P-T) points, ranging from 0-140 GPa and 300-3000 K, thus covering the P-T conditions of the lower mantle (Table 1). Axial ratios b/a and c/a follow smooth trends at lower mantle pressures (Figures 3a-3b), with deviations away from the $Pbnm$ structure seen at $P \leq 12$ GPa and $T \geq 2400$ K. At 3000 K and 12 GPa the structure can be observed to move towards cubic lattice parameters ($b/a \rightarrow 1$, $c/a \rightarrow \sqrt{2}$). This point, in particular, is close to the melting curve of Mg-pv [Heinz and Jeanloz, 1987; Knittle and Jeanloz 1989; Poirier, 1989], and such temperature-induced phase transitions have been predicted for Mg-pv by MD [Wolf and Bukowinski, 1987] and lattice dynamics [Matsui and Price, 1991]. In addition, it has been found for RbCaF₃ and KMnF₃ perovskites by MD simulations [Lewis and Lépine, 1989; Nosé and Klein, 1989] and observed experimentally in the fluoride perovskite neighborite (NaMgF₃) [Chao et al., 1961]. Regardless of these changes, the volumes are well-behaved as functions of pressure and temperature (Figure 3c), and no other structural anomalies or melting was encountered during runs at other P-T points.

The resulting P-V-T EOS fits and their reduced χ^2 values are given in Table 2. Both the Birch-Murnaghan and Universal EOSs are in excellent agreement with experimental results. As for the accuracy

of our thermal pressure expression, RMS differences between volumes found using equation (1) for either EOS and those found using isothermal EOSs are of the order of 10^{-3} \AA^3 . As for the differences between the two equation of state forms, Jeanloz [1988] compared them over moderate compressions and found that they are quite similar. More recent work by Cohen et al. [2000] supports this, but they found that for large (>30%) strains and for determining parameters such as V_0 , K_{T_0} , and K'_{T_0} , the Universal EOS works best. So, for the rest of our analyses we use that here. However, given that under the pressure range studied, compressions will be no greater than 25%, so we can confidently compare our results with those of others that were found with the Birch-Murnaghan EOS.

Once we determined the EOS parameters, we determined volumes for Mg-pv over a wide P-T range (-10-150 GPa, 0-3300 K). Using this extended data set, we determined the isothermal bulk modulus [$K_T = -V(\partial P/\partial V)_T$] at those points and α , δ_T , γ , and q using equations (7), (8), (11), and (10). We found $(\partial K/\partial T)_{P=0} = -0.0251 \text{ GPa K}^{-1}$, close to those found experimentally, $-0.023 \text{ GPa K}^{-1}$ [Wang et al., 1994] and $-0.027 \text{ GPa K}^{-1}$ [Fiquet et al., 1998], as well as one found by the inversion of multiple experimental data sets, $-0.021 \text{ GPa K}^{-1}$ [Jackson and Rigden, 1996].

Figure 4 shows α at pressures from 0 to 140 GPa. Experimental results shown have higher T slopes, as well as higher extrapolated values for most temperatures, though an average value found by Jackson and Rigden [1996] at zero GPa of $2.6 \times 10^{-5} \text{ K}^{-1}$ over 300-1660 K matches our value over the same T range exactly. Kato et al. [1995] found an average value of $2.0 \pm 0.4 \times 10^{-5} \text{ K}^{-1}$ over 298-1473 K and 25 GPa, close to our average value of $1.89 \times 10^{-5} \text{ K}^{-1}$ at the same conditions. The lack of quantum effects in our MD results can be seen at low temperatures; instead of tending toward zero at zero temperature, α remains large. The δ_T increases with T , but decreases as P increases (Figure 5). The dependency of δ_T on T decreases as a function of P , with convergence to a value of 2.87 at ~ 130 GPa, similar to the high-pressure behavior in MgO found by the same MD method [Inbar and Cohen, 1995]. Our value of $\delta_T = 3.79$ at ambient conditions is in excellent agreement with the experimentally derived value of Wang et al. [1994] of 3.73, though it is lower than the value of 4.5, found by Masuda and Anderson [1995] from the experimental data of Utsumi et al. [1995]. Other theoretical determinations of δ_T are much higher, however. Hama

Figure 4

Figure 5

and Suito [1998a] found a value of 5.21, on the basis of calculations using the LAPW results of *Stixrude and Cohen* [1993] and the Debye approximation for lattice vibration. Using MD and semiempirical potentials [Matsui, 1988], *Belonoshko and Dubrovinsky* [1996] found $\delta_T = 5.80$, and *Patel et al.* [1996] found $\delta_T = 7.0$ using the same potentials, combining MD with lattice dynamics. *Anderson* [1998], using Debye theory, calculated zero pressure values ranging from 4.98 at 400 K to ~ 4 at $1000 \text{ K} \leq T \leq 1800 \text{ K}$, coming close to our values at those temperatures.

The Grüneisen parameter also increases as a function of T and decreases as a function of P and approaches a value of 1 at pressures of 130-140 GPa (Figure 6). Our value of 1.33 at zero P and 300 K matches well with *Wang et al.*'s [1994] value of 1.3 and *Utsumi et al.*'s [1995] and *Masuda and Anderson's* [1995] value of 1.45. *Stixrude et al.* [1992], using the experimental data of *Mao et al.* [1991], found a higher value of $\gamma = 1.96$. Values determined by the inversion of multiple experimentally determined P-V-T data sets match well also: 1.5 [Bina, 1995], 1.33 [Jackson and Rigden, 1996], and 1.42 [Shim and Duffy, 2000]. Two shock wave studies find a value of 1.5 [Duffy and Ahrens, 1993; Akins and Ahrens, 1999] on the basis of limited data sets: four for the former (with q fixed equal to 1) and two for the latter. Values of γ from theoretical studies range from very close to ours, 1.279 [Hama and Suito, 1998a] and 1.44 [Hemley et al., 1987], to 1.97 [Belonoshko and Dubrovinsky, 1996; Patel et al., 1996]. *Anderson's* [1998] zero pressure, 300 K value of 1.52 is somewhat higher than ours, but at 400-1800 K his values of ~ 1.4 are very close to ours.

The volume dependence of γ , q , is 1.03 at 300 K (Figure 7). Our equation of state form, with ΔP_{th} linear in T and independent of volume, constrains $q = 1$ if the isochoric heat capacity $C_V = 3nR$, the classical harmonic value. As T increases, we find that q increases to a value of 1.07 at 3000 K owing to anharmonicity. Values from inverted experimental data sets range from 1.0 [Bina, 1995] to 2.0 [Shim and Duffy, 2000]. *Stixrude et al.* [1992] found a high q value of 2.5 to go along with their value for γ . *Akins and Ahrens's* [1999] value was even higher, $q = 4.0 \pm 1.0$ with $C_V = 5nR$, but these are preliminary conclusions based on limited data. *Patel et al.* [1996] found a value of 3.0 at 0 GPa, decreasing to 1.7 at 100 GPa using a combination of molecular and lattice dynamics. *Anderson's* [1998] Debye calculations gave values close to unity at $T \geq 1000 \text{ K}$, with q decreasing

slightly with increasing T , to 0.82 at 1800 K.

4. Discussion and Conclusions

Taking sets of experimental P-V-T data, we fit the high temperature data [Fiquet et al., 1998, 2000; Saxena et al., 1999] and available experimental MgSiO₃ data to our thermal Universal EOS form (Table 2) in order to have consistent bases for comparison. The resulting fits have higher statistical uncertainties but compare well with our results. Volumes calculated along the lower mantle geothermal gradient of *Brown and Shankland* [1981], which has a starting T of 1873 K at 670 km (Figure 1), show that those calculated from our EOS are 3 to 4 Å³ per unit cell larger, $\sim 2.5\%$, than those calculated from the inverted experimental data sets (Figure 8). This corresponds to density differences of $\sim 0.1 \text{ g cm}^{-3}$. This is the opposite of the typical error of the local density approximation to density functional theory, on which our method is based. The larger volume is due to the choice of ionic charges and other model assumptions. If we fix V_0 to the experimentally determined value of 162.49 Å³ [Mao et al., 1991] but otherwise use our EOS parameters, our calculated volumes are very close, within 1%, to the volumes derived from the inverted experimental data sets. The comparisons also improve as pressure increases. To compare our model with other zero temperature theoretically derived EOSs, we calculated volumes at 0 K from 0-140 GPa and fit an isothermal Universal EOS to them (Table 3).

Compositional models of the lower mantle can be tested against seismological models by examining densities and seismic wave velocities as functions of depth. Candidates include pyrolite [Ringwood, 1975] and chondritic or pure perovskite models. Studies support both the former [Bina and Silver, 1990; Stacey, 1996] and latter [Butler and Anderson, 1978; Stixrude et al., 1992], though uncertainties in the thermodynamic parameters of the constituent minerals make it difficult to resolve this question with certainty. Indeed, several studies have been able to support both models depending on whether high (pure perovskite) or low (pyrolite) values of α and δ_T or γ and q are used [Zhao and Anderson, 1994; Anderson et al., 1995; Karki and Stixrude, 1999].

Calculating the densities of Mg-pv along a geothermal gradient [Brown and Shankland, 1981] (Figure 9a), we see that they are $\sim 0.2\text{-}0.3 \text{ g cm}^{-3}$ ($\sim 4\text{-}5\%$) too low compared with those from the Prelim-

Figure 8

Table 3

Figure 9

inary Reference Earth Model (PREM) [Dziewonski and Anderson, 1981]. The calculated bulk sound velocities, $V_\varphi = \sqrt{K_S/\rho}$, where $K_S = K_T(1 + \gamma\alpha T)$, are, in turn, $\sim 0.4\text{-}0.6 \text{ km s}^{-1}$ ($\sim 4\text{-}7\%$) too high compared to the ak135-f seismological model [Kennett et al., 1995; Montagner and Kennett, 1996] (Figure 9b). Using the experimentally determined value of $V_0 = 162.49 \text{ \AA}^3$ [Mao et al., 1991] in place of our calculated value does increase the densities somewhat, but not enough to match the PREM values.

As the perovskite found in the lower mantle should be a solid solution of the Mg and Fe end-members, we added iron by adjusting density by [Jeanloz and Thompson, 1983],

$$\rho(X_{\text{Fe}}) = \rho(0)(1 + 0.269 X_{\text{Fe}}) \quad (12)$$

but we did not change the bulk moduli [Mao et al., 1991]. Including 10 mol % Fe does cause densities to agree somewhat with the PREM values (Figure 10a), but the bulk sound velocities are still much too high (Figure 10b). Consequently, we find that the lower mantle cannot consist solely of (Mg,Fe)SiO₃ perovskite.

We also tested pyrolitic compositions consisting of mixtures of perovskite and magnesiowüstite (mw). Densities of mw were calculated using the thermodynamic data set of Fei et al. [1991], as well as K_T s for the Mg end-member. K_S s were then calculated using the relation

$$\alpha(P, T) = \alpha(P_0, T) \left[\frac{V(P, T)}{V(P_0, T)} \right]^{\delta_T}, \quad (13)$$

with δ_T and γ from Inbar and Cohen [1995]. Iron was accounted for in K_S via the relationship [Jeanloz and Thompson, 1983]

$$K_S(X_{\text{Fe}}) = K_S(0) + 17 X_{\text{Fe}}. \quad (14)$$

$X_{\text{Mg}} = 0.93\text{-}0.96$ for perovskite (pv) and $0.82\text{-}0.86$ for mw [Katsura and Ito, 1996; Martinez et al., 1997] were used. Densities and bulk sound velocities were calculated using Voigt-Reuss-Hill averaging for two simplified pyrolite models (high [1] and low [2] Fe content) consisting of 67 vol % pv and 33 vol % mw and were found to be in excellent agreement with the seismological models (Figure 11). The two pyrolite models have partitioning coefficients $K_{\text{Fe-Mg}}^{\text{pv-mw}}$ of 0.34 and 0.26, where

$$K_{\text{Fe-Mg}}^{\text{pv-mw}} = \frac{X_{\text{Fe}}^{\text{pv}}/X_{\text{Mg}}^{\text{pv}}}{X_{\text{Fe}}^{\text{mw}}/X_{\text{Mg}}^{\text{mw}}}. \quad (15)$$

Experimental evidence suggests that for such a bulk composition, $K_{\text{Fe-Mg}}^{\text{pv-mw}}$ should increase in the mantle from ~ 0.20 (660 km) to ~ 0.35 (1500 km), with $X_{\text{Mg}}^{\text{pv}}$ decreasing and $X_{\text{Mg}}^{\text{mw}}$ increasing with depth [Mao et al., 1997]. Compositional models with high Fe content of pv and low Fe content of mw (and vice versa) fall inbetween the results of those shown in Figure 11. Given the range of Fe-Mg partitioning between perovskite and magnesiowüstite under the appropriate pressure and temperature conditions, we find pyrolite to be the most likely compositional model for the lower mantle.

Given that other components (Al, Fe³⁺) and phases (CaSiO₃ perovskite) should be present in the lower mantle, we do not expect exact agreement of a simplified pyrolite model with any seismological model. It is believed that, under lower mantle conditions, Al₂O₃ is mainly incorporated into the Mg-pv structure [Irifune, 1994; Wood, 2000]. Generally, the effect of the incorporation of Al into Mg-pv on its physical properties has been considered small [e.g., Weidner and Wang, 1998]. However, Al, unlike Fe, causes significant distortion in the Mg-pv lattice [O'Neill and Jeanloz, 1994], which may affect the compressibility. Recent experimental work by Zhang and Weidner [1999], at pressure of up to 10 GPa and temperatures of up to 1073 K, indicates that compared with MgSiO₃, Mg-pv with 5 mol % Al has a smaller K_T value (232-236 GPa) and a $(\partial K_T/\partial T)_P$ value more than double that in magnitude. The values for α_0 , $(\partial\alpha/\partial T)_P$, and δ_T are also larger. Smaller bulk moduli and the higher density (0.2% at 300 K and 0 GPa) would cause seismic velocities to decrease. In addition, the presence of Al tends to equalize the partitioning of Fe into perovskite and magnesiowüstite and may allow garnet to coexist with perovskite in the uppermost ~ 100 km of the lower mantle [Wood and Rubie, 1996; Wood, 2000]. These partitioning experiments, however, were done at high f_{O_2} , so it is uncertain how applicable they are to the mantle. The effect of the presence of Fe³⁺ in Mg-pv on the EOS and elasticity, while known for defect concentrations and electrostatic charge balance [McCammon, 1997, 1998], is unknown. As for CaSiO₃ perovskite (Ca-pv), experimental data suggest that its elastic properties are in excellent agreement with seismological models and thus would be invisible in the lower mantle [Wang et al., 1996; Hama and Suito, 1998b].

Performing MD calculations over the range pressures and temperatures found in the Earth's mantle, we find a thermal EOS that is in excellent agreement

with experimental results. Thermodynamic parameters can be derived that agree well with experimentally determined values and that can be confidently interpolated to conditions found in the lower mantle. Moreover, no solid-solid phase transitions or melting was found during the runs under lower mantle conditions, so orthorhombic MgSiO_3 perovskite should be stable to the core-mantle boundary. Using these results, we find that pyrolite with $K_{\text{Fe-Mg}}^{\text{PV-mw}} = 0.26\text{-}0.34$ is the most likely compositional model for the lower mantle.

Acknowledgments. We thank Iris Inbar, Russell Hemley, Stephen Gramsch, Joe Akins, Mark Woods, Sheila Coleman, and Lars Stixrude for helpful discussions and comments. We acknowledge the support of the National Science Foundation through grant EAR-9870328. The computations were performed on the Cray SV1 at the Geophysical Laboratory, with the support of NSF grant EAR-9975753 and the W. M. Keck Foundation.

References

- Akins, J. A., and T. J. Ahrens, Shock wave equation of state measurements on MgSiO_3 perovskite at lower mantle pressures indicate $\gamma_0 = 1.5$ and $q = \partial \ln \gamma / \partial \ln V > 3$, *Eos Trans. AGU*, 80 (46), Fall Meet. Suppl., F757, 1999.
- Anderson, O. L., An experimental high-temperature thermal equation of state bypassing the Grüneisen parameter, *Phys. Earth Planet. Inter.*, 1, 173-183, 1980.
- Anderson, O. L., A universal thermal equation-of-state, *J. Geodyn.*, 1, 185-214, 1984.
- Anderson, O. L., Thermoelastic properties of MgSiO_3 perovskite using the Debye approach, *Am. Mineral.*, 83, 23-35, 1998.
- Anderson, O. L., and I. Suzuki, Anharmonicity of three minerals at high temperature: Forsterite, fayalite, and periclase, *J. Geophys. Res.*, 88, 3549-3356, 1983.
- Anderson, O. L., K. Masuda, and D. Guo, Pure silicate perovskite and the PREM lower mantle model: a thermodynamic analysis, *Phys. Earth Planet. Inter.*, 89, 35-49, 1995.
- Belonoshko, A. B., Molecular dynamics of MgSiO_3 perovskite at high pressures: Equation of state, structure, and melting transition, *Geochim. Cosmochim. Acta*, 58, 4039-4047, 1994.
- Belonoshko, A. B., and L. S. Dubrovinsky, Equations of state of MgSiO_3 -perovskite and MgO (periclase) from computer simulations, *Phys. Earth Planet. Inter.*, 98, 47-54, 1996.
- Bina, C. R., Confidence limits for silicate perovskite equations of state, *Phys. Chem. Miner.*, 22, 375-382, 1995.
- Bina, C. R., Lower mantle mineralogy and the geophysical perspective, *Rev. Mineral.*, 37, 205-239, 1998.
- Bina, C. R., and P. G. Silver, Constraints on lower mantle composition and temperature from density and bulk sound velocity profiles, *Geophys. Res. Lett.*, 17, 1153-1156, 1990.
- Birch, F., Elasticity and constitution of the Earth's interior, *J. Geophys. Res.*, 57, 227-286, 1952.
- Brown, J. M., and T. J. Shankland, Thermodynamic parameters in the Earth as determined from seismic profiles, *Geophys. J. R. Astron. Soc.*, 66, 579-596, 1981.
- Butler, R., and D. L. Anderson, Equations of state fits to the lower mantle and outer core, *Phys. Earth Planet. Inter.*, 17, 147-162, 1978.
- Chao, E. C. T., H. T. Evans, B. J. Skinner, and C. Milton, Neighborite, NaMgF_3 , a new mineral from the Green River Formation, South Ouray, Utah, *Am. Mineral.*, 46, 379-393, 1961.
- Cohen, R. E., Elasticity and equation of state of MgSiO_3 perovskite, *Geophys. Res. Lett.*, 14, 1053-1056, 1987.
- Cohen, R. E., L. L. Boyer, M. J. Mehl, W. E. Pickett, and H. Krakauer, Electronic structure and total energy calculations for oxide perovskites and superconductors, in *Perovskite: A Structure of Great Interest to Geophysics and Materials Science*, *Geophys. Monogr. Ser.*, 45, edited by A. Navrotsky and D. J. Weidner, pp. 55-66, AGU, Washington, D. C., 1989.
- Cohen, R. E., O. Gülsersen, and R. J. Hemley, Accuracy of equation-of-state formulations, *Am. Mineral.*, 85, 338-344, 2000.
- Dubrovinsky, L., S. K. Saxena, R. Ahuja, and B. Johansson, Theoretical study of the stability of MgSiO_3 -perovskite in the deep mantle, *Geophys. Res. Lett.*, 25, 4253-4256, 1998.
- Duffy, T. S., and T. J. Ahrens, Thermal properties of perovskite above 100 GPa from shock and static compression data, *Eos Trans. AGU*, 74 (43), Fall Meet. Suppl., 571, 1993.
- Dziewonski, A. M., and D. L. Anderson, Preliminary reference Earth model, *Phys. Earth Planet. Inter.*, 25, 297-356, 1981.
- Fei, Y., H. K. Mao, and B. O. Mysen, Experimental determination of element partitioning and calculation of phase relations in the MgO-FeO-SiO_2 system at high pressure and high temperature, *J. Geophys. Res.*, 96, 2157-2169, 1991.
- Fiquet, G., D. Andrault, A. Dewaele, T. Charpin, M. Kunz, and D. Häusermann, P-V-T equation of state of MgSiO_3 perovskite, *Phys. Earth Planet. Inter.*, 105, 21-31, 1998.
- Fiquet, G., A. Dewaele, D. Andrault, M. Kunz, and T. Le Bihan, Thermoelastic properties and crystal structure of MgSiO_3 perovskite at lower mantle pressure and temperature conditions, *Geophys. Res. Lett.*, 27, 21-24, 2000.

- Funamori, N., T. Yagi, W. Utsumi, T. Kondo, and T. Uchida, Thermoelastic properties of MgSiO_3 perovskite determined by in situ X ray observations up to 30 GPa and 2000 K, *J. Geophys. Res.*, *101*, 8257-8269, 1996.
- Gear, C. W., *Numerical Initial Value Problems in Ordinary Differential Equations*, 253 pp., Prentice-Hall, Old Tappan, N. J., 1971.
- Gordon, R. G., and Y. S. Kim, Theory for the forces between closed-shell atoms and molecules, *J. Chem. Phys.*, *56*, 3122-3133, 1972.
- Hama, J., and K. Suito, Equation of state of MgSiO_3 perovskite and its thermoelastic properties under lower mantle conditions, *J. Geophys. Res.*, *103*, 7443-7462, 1998a.
- Hama, J., and K. Suito, High-temperature equation of state of CaSiO_3 perovskite and its implications for the lower mantle conditions, *Phys. Earth Planet. Inter.*, *105*, 33-46, 1998b.
- Hedin, L., and B. I. Lundqvist, Explicit local-exchange correlation potentials, *J. Phys. C. Solid State Phys.*, *4*, 2064-2083, 1971.
- Heinz, D. L., and R. Jeanloz, Measurement of the melting curve of $\text{Mg}_{0.9}\text{Fe}_{0.1}\text{SiO}_3$ at lower mantle conditions and its geophysical implications, *J. Geophys. Res.*, *92*, 11,437-11,444, 1987.
- Hemley, R. J., and R. E. Cohen, Structure and bonding in the deep mantle and core, *Philos. Trans. R. Soc. London, Ser. A*, *354*, 1461-1479, 1996.
- Hemley, R. J., M. D. Jackson, and G. G. Gordon, Theoretical study of the structure, lattice dynamics, and equations of state of perovskite-type MgSiO_3 and CaSiO_3 , *Phys. Chem. Miner.*, *14*, 2-12, 1987.
- Inbar, I., and R. E. Cohen, High pressure effects on thermal properties of MgO , *Geophys. Res. Lett.*, *22*, 1533-1536, 1995.
- Irifune, T., Absence of an aluminous phase in the upper part of the Earth's lower mantle, *Nature*, *370*, 131-133, 1994.
- Jackson, I., and S. M. Rigden, Analysis of P-V-T data: Constraints on the thermoelastic properties of high-pressure minerals, *Phys. Earth Planet. Inter.*, *96*, 85-112, 1996.
- Jeanloz, R., Universal equation of state, *Phys. Rev. B Condens. Matter*, *38*, 805-807, 1988.
- Jeanloz, R., and A. B. Thompson, Phase transitions and mantle discontinuities, *Rev. Geophys.*, *21*, 51-74, 1983.
- Karki, B. B., and L. Stixrude, Seismic velocities of major silicate and oxide phases of the lower mantle, *J. Geophys. Res.*, *104*, 13,025-13,033, 1999.
- Karki, B. B., L. Stixrude, S. J. Clark, M. C. Warren, G. J. Ackland, and J. Crain, Elastic properties of orthorhombic MgSiO_3 perovskite at lower mantle pressures, *Am. Mineral.*, *82*, 635-638, 1997.
- Kato, T., E. Ohtani, H. Morishima, D. Yamazaki, A. Suzuki, M. Suto, T. Kubo, T. Kikegawa, and O. Shimomura, In situ X ray observation of high-pressure phase transitions of MgSiO_3 and thermal expansion of MgSiO_3 perovskite at 25 GPa by double-stage multianvil system, *J. Geophys. Res.*, *100*, 20,475-20,481, 1995.
- Katsura, T., and E. Ito, Determination of Fe-Mg partitioning between perovskite and magnesiowüstite, *Geophys. Res. Lett.*, *23*, 2005-2008, 1996.
- Kennett, B. L. N., E. R. Engdahl, and R. Buland, Constraints on seismic velocities in the Earth from travel-times, *Geophys. J. Int.*, *122*, 108-124, 1995.
- Knittle, E., and R. Jeanloz, Synthesis and equation of state of $(\text{Mg,Fe})\text{SiO}_3$ perovskite to over 100 gigapascals, *Science*, *235*, 668-670, 1987.
- Knittle, E., and R. Jeanloz, Melting curve of $(\text{Mg,Fe})\text{SiO}_3$ perovskite to 96 GPa: Evidence for a structural transition in lower mantle melts, *Geophys. Res. Lett.*, *16*, 421-424, 1989.
- Kudoh, Y., E. Ito, and H. Takeda, Effect of pressure on the crystal structure of perovskite-type MgSiO_3 , *Phys. Chem. Miner.*, *14*, 350-354, 1987.
- Lewis, L. J., and Y. Lépine, Structural transitions in fluorine-based perovskites: A molecular dynamics study of KMnF_3 , *Phys. Rev. B Condens. Matter*, *40*, 3319-3322, 1989.
- Mao, H. K., R. J. Hemley, Y. Fei, J. F. Shu, L. C. Chen, A. P. Jephcoat, and Y. Wu, Effect of pressure, temperature, and composition on lattice parameters and density of $(\text{Fe,Mg})\text{SiO}_3$ -perovskites to 30 GPa, *J. Geophys. Res.*, *96*, 8069-8079, 1991.
- Mao, H. K., G. Shen, and R. J. Hemley, Multivariable dependence of Fe-Mg partitioning in the lower mantle, *Science*, *278*, 2098-2100, 1997.
- Martinez, I., Y. Wang, F. Guyot, R. C. Liebermann, and J. C. Doukhan, Microstructures and iron partitioning in $(\text{Mg,Fe})\text{SiO}_3$ perovskite - $(\text{Mg,Fe})\text{O}$ magnesiowüstite assemblages: An analytical transmission electron microscopy study, *J. Geophys. Res.*, *102*, 5265-5280, 1997.
- Martyna, G. J., D. J. Tobias, and M. L. Klein, Constant pressure molecular dynamics algorithms, *J. Chem. Phys.*, *101*, 4177-4189, 1994.
- Masuda, K., and O. L. Anderson, The isentropic density profile of silicate perovskite computed by thermal pressure, *Geophys. Res. Lett.*, *22*, 2211-2214, 1995.
- Matsui, M., Molecular dynamics study of MgSiO_3 perovskite, *Phys. Chem. Miner.*, *16*, 234-238, 1988.
- Matsui, M., and G. D. Price, Simulation of the pre-melting behaviour of MgSiO_3 perovskite at high pressures and temperatures, *Nature*, *351*, 735-737, 1991.
- McCammon, C., Perovskite as a possible sink for ferric iron in the lower mantle, *Nature*, *387*, 694-696, 1997.

- McCammon, C., The crystal chemistry of ferric iron in $\text{Fe}_{0.05}\text{Mg}_{0.95}\text{SiO}_3$ perovskite as determined by Mössbauer spectroscopy in the temperature range 80-293 K, *Phys. Chem. Miner.*, *25*, 292-300, 1998.
- Meade, C., H. K. Mao, and J. Hu, High-temperature phase transition and dissociation of $(\text{Mg,Fe})\text{SiO}_3$ perovskite at lower mantle pressures, *Science*, *268*, 1743-1745, 1995.
- Montagner, J.-P., and B. L. N. Kennett, How to reconcile body-wave and normal-mode reference earth models, *Geophys. J. Int.*, *125*, 229-248, 1996.
- Nosé, S., and M. L. Klein, Structure and dynamics of the fluorperovskite, RbCaF_3 , *J. Chem. Phys.*, *90*, 5005-5010, 1989.
- O'Neill, B., and R. Jeanloz, MgSiO_3 - FeSiO_3 - Al_2O_3 in the Earth's lower mantle: Perovskite and garnet at 1200 km depth, *J. Geophys. Res.*, *99*, 19,901-19,915, 1994.
- Patel, A., G. D. Price, M. Matsui, J. P. Brodholt, and R. J. Howarth, A computer simulation approach to the high pressure thermoelasticity of MgSiO_3 perovskite, *Phys. Earth Planet. Inter.*, *98*, 55-63, 1996.
- Poirier, J. P., Lindemann law and the melting temperature of perovskites, *Phys. Earth Planet. Inter.*, *54*, 364-369, 1989.
- Ringwood, A. E., *Composition and Petrology of the Earth's Mantle*, 618 pp., McGraw-Hill, New York, 1975.
- Ross, N. L., and R. M. Hazen, High-pressure crystal chemistry of MgSiO_3 perovskite, *Phys. Chem. Miner.*, *17*, 228-237, 1990.
- Saxena, S. K., L. S. Dubrovinsky, P. Lazor, Y. Cerenius, P. Häggkvist, M. Hanfland, and J. Hu, Stability of perovskite (MgSiO_3) in the Earth's mantle, *Science*, *274*, 1357-1359, 1996.
- Saxena, S. K., L. S. Dubrovinsky, P. Lazor, and J. Hu, In situ X-ray study of perovskite (MgSiO_3): Phase transition and dissociation at mantle conditions, *Eur. J. Mineral.*, *10*, 1275-1281, 1998.
- Saxena, S. K., L. S. Dubrovinsky, F. Tutti, and T. Le Bihan, Equation of state of MgSiO_3 with the perovskite structure based on experimental measurement, *Am. Mineral.*, *84*, 226-232, 1999.
- Serghiou, G., A. Zerr, and R. Boehler, $(\text{Mg,Fe})\text{SiO}_3$ -perovskite stability under lower mantle conditions, *Science*, *280*, 2093-2095, 1998.
- Shim, S.-H., and T. S. Duffy, Constraints on the P-V-T equation of state of MgSiO_3 perovskite, *Am. Mineral.*, *85*, 354-363, 2000.
- Stacey, F. D., Thermoelasticity of $(\text{Mg,Fe})\text{SiO}_3$ perovskite and a comparison with the lower mantle, *Phys. Earth Planet. Inter.*, *98*, 65-77, 1996.
- Stixrude, L., and M. S. T. Bukowinski, Stability of $(\text{Mg,Fe})\text{SiO}_3$ perovskite and the structure of the lowermost mantle, *Geophys. Res. Lett.*, *19*, 1057-1060, 1992.
- Stixrude, L., and R. E. Cohen, Stability of orthorhombic MgSiO_3 perovskite in the Earth's lower mantle, *Nature*, *364*, 613-616, 1993.
- Stixrude, L., R. J. Hemley, Y. Fei, and H. K. Mao, Thermoelasticity of silicate perovskite and magnesiowüstite and stratification of the Earth's mantle, *Science*, *257*, 1099-1101, 1992.
- Utsumi, W., N. Funamori, T. Yagi, E. Ito, T. Kikegawa, and O. Shimomura, Thermal expansivity of MgSiO_3 perovskite under high pressures up to 20 GPa, *Geophys. Res. Lett.*, *22*, 1005-1008, 1995.
- Vinet, P., J. Ferrante, J. H. Rose, and J. R. Smith, Compressibility of solids, *J. Geophys. Res.*, *92*, 9319-9325, 1987.
- Wang, Y., D. J. Weidner, R. C. Liebermann, and Y. Zhao, P-V-T equation of state of $(\text{Mg,Fe})\text{SiO}_3$ perovskite: Constraints on composition of the lower mantle, *Phys. Earth Planet. Inter.*, *83*, 13-40, 1994.
- Wang, Y., D. J. Weidner, and F. Guyot, Thermal equation of state of CaSiO_3 perovskite, *J. Geophys. Res.*, *101*, 661-672, 1996.
- Weidner, D. J., and Y. Wang, Chemical- and Clapeyron-induced buoyancy at the 660 km discontinuity, *J. Geophys. Res.*, *103*, 7431-7441, 1998.
- Wentzcovitch, R. M., N. L. Ross, and G. D. Price, Ab initio study of MgSiO_3 and CaSiO_3 perovskites at lower-mantle pressures, *Phys. Earth Planet. Inter.*, *90*, 101-112, 1995.
- Wolf, G. H., and M. S. T. Bukowinski, Theoretical study of the structural properties and equations of state of MgSiO_3 and CaSiO_3 perovskites: Implications for lower mantle composition, in *High-Pressure Research in Mineral Physics*, *Geophys. Monogr. Ser.*, *39*, edited by M. H. Manghnani and Y. Syono, pp. 313-331, AGU, Washington, D. C., 1987.
- Wolf, G. H., and M. S. T. Bukowinski, Variational stabilization of the ionic charge densities in the electron-gas theory of crystals: Applications to MgO and CaO , *Phys. Chem. Minerals*, *15*, 209-220, 1988.
- Wood, B. J., Phase transformations and partitioning relations in peridotite under lower mantle conditions, *Earth Planet. Sci. Lett.*, *174*, 341-354, 2000.
- Wood, B. J., and D. C. Rubie, The effect of alumina on phase transformations at the 660 kilometer discontinuity from Fe-Mg partitioning effects, *Science*, *273*, 1522-1524, 1996.
- Yeganeh-Haeri, A., Synthesis and re-investigation of the elastic properties of single-crystal magnesium silicate perovskite, *Phys. Earth Planet. Inter.*, *87*, 111-121, 1994.
- Zhang, J., and D. J. Weidner, Thermal equation of state of aluminum-enriched silicate perovskite, *Science*, *284*, 782-784, 1999.

Zhao, Y., and D. L. Anderson, Mineral physics constraints on the chemical composition of the Earth's lower mantle, *Phys. Earth Planet. Inter.*, 85, 273-292, 1994.

R. E. Cohen, and F. C. Marton, Geophysical Laboratory and Center for High Pressure Research, Carnegie Institution of Washington, 5251 Broad Branch Road, NW, Washington, D. C. 20015-1305. (cohen@gl.ciw.edu; marton@gl.ciw.edu)

J. Ita, Shell International Exploration and Production, P. O. Box 60, Rijswijk, 2280 AB, Netherlands. (j.j.ita@siep.shell.com)

Received March 29, 2000; revised September 28, 2000; accepted December 5, 2000.

¹Now at Shell International Exploration and Production, Rijswijk, Netherlands.

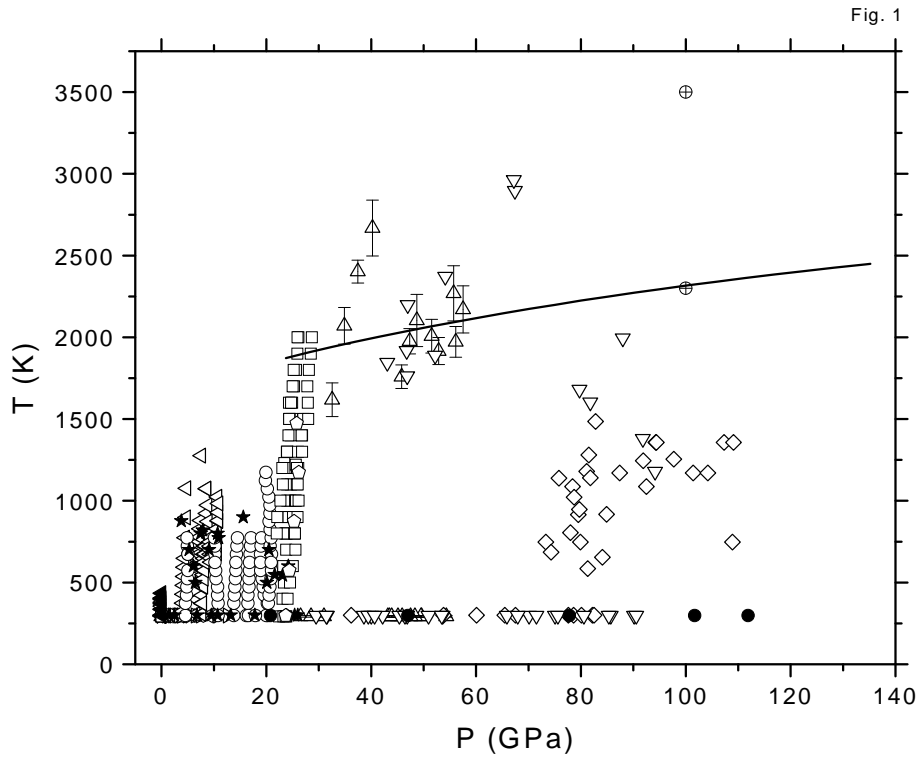


Figure 1. Experimental pressure-temperature coverage of $(\text{Mg,Fe})\text{SiO}_3$ perovskite. Open symbols are for static experiments on $X_{\text{Mg}} = 1.0$, solid symbols are for $X_{\text{Mg}} = 0.9$, and open symbols with crosses are shock wave data. Hexagons, *Kudoh et al.*, [1987]; right-facing triangles, *Ross and Hazen*, [1990]; left-facing triangles, *Wang et al.*, [1994]; upward pointing triangles, *Fiquet et al.*, [1998]; downward pointing triangles, *Fiquet et al.*, [2000]; diamonds, *Saxena et al.*, [1999]; open circles, *Utsumi et al.*, [1995]; solid circles, *Knittle and Jeanloz*, [1987]; squares, *Funamori et al.*, [1996]; stars, *Mao et al.*, [1991]; pentagons, *Kato et al.*, [1995]; circle with cross, *Duffy and Ahrens*, [1993]. Solid curve is the lower mantle geothermal gradient of *Brown and Shankland* [1981]. Static experimental work has direct coverage of approximately the upper one third. The shock wave data point that falls near the geotherm is perovskite plus magnesiowüstite.

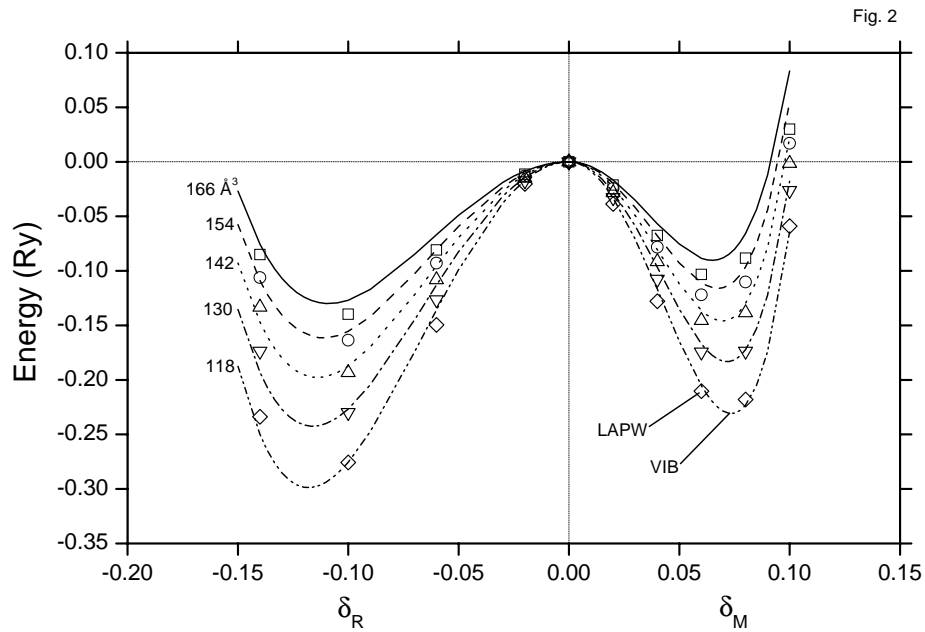
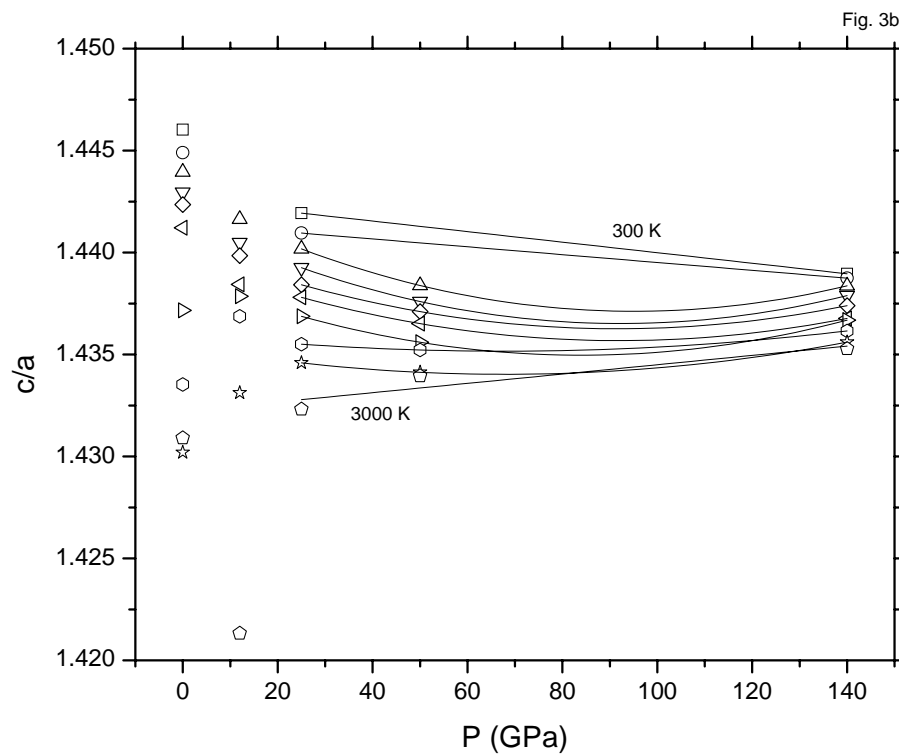
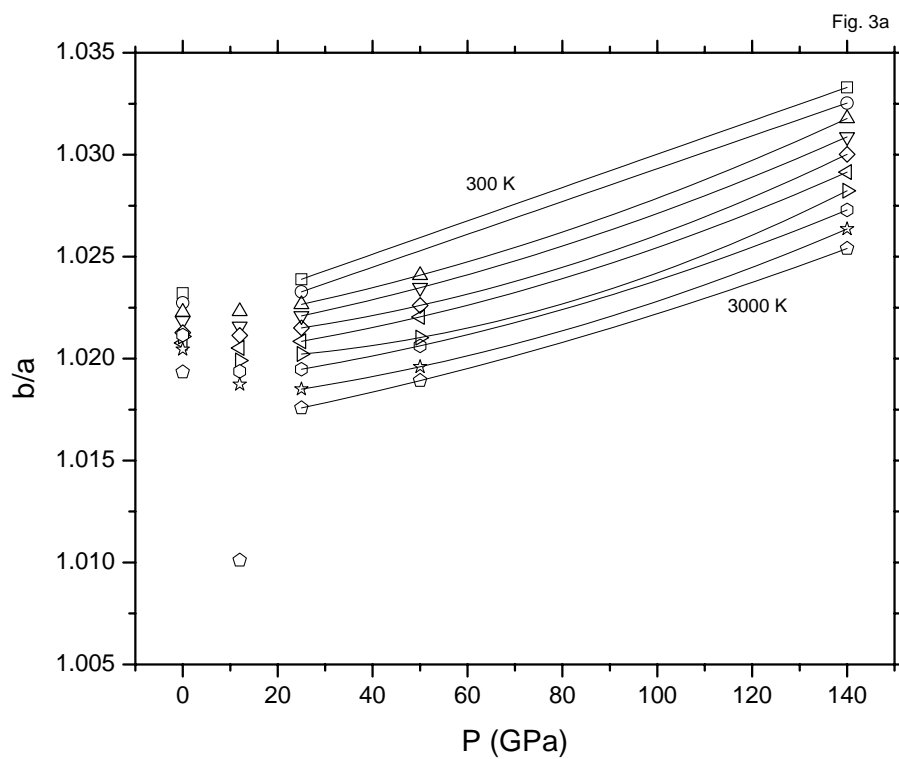


Figure 2. Energetics of octahedral rotations: calculated total energies relative to the cubic structure ($Pm3m$) using VIB (curves) and LAPW [Stixrude and Cohen, 1993; Hemley and Cohen, 1996] (symbols) as a function of (left) R and (right) M point rotation angles as represented by the fractional change in the oxygen coordinate (δ_R and δ_M). The orthorhombic structure ($Pbnm$) occurs at $\delta_R = 0.0912$ and $\delta_M = 0.0766$ at $P = 0$ GPa.



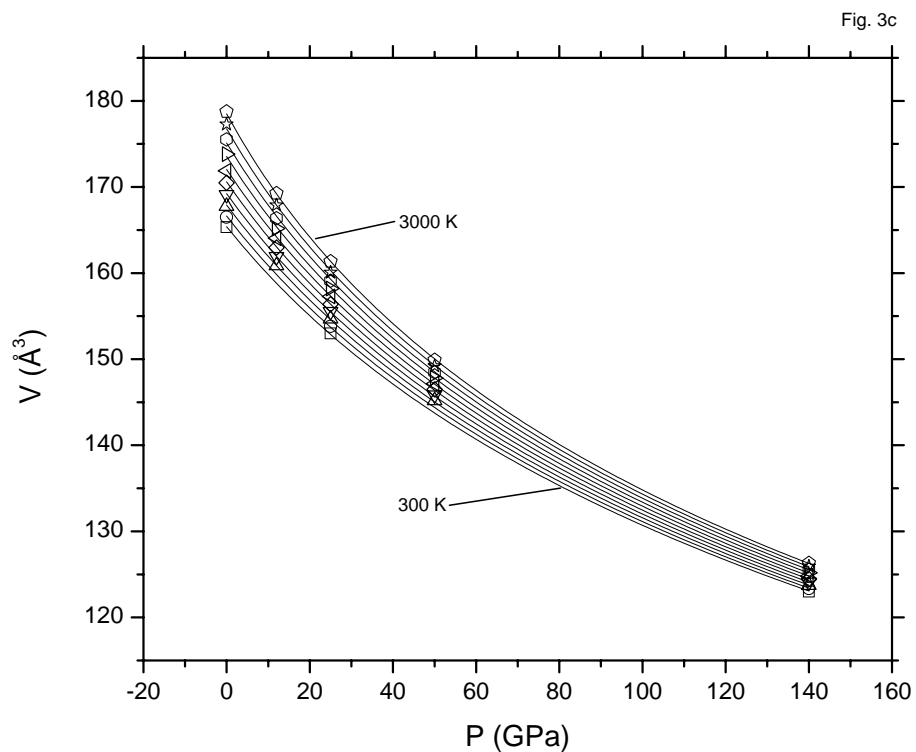


Figure 3. Structural parameters and volumes of MD results: (a) b/a axis ratio and (b) c/a axis ratio. At low pressures and high temperatures the structure begins to deviate from orthorhombic $Pbnm$, but no phase transitions, with the possibility of the structure heading toward cubic at 12 GPa and 3000 K. (c) Volume. Symbols are MD results and curves are Universal EOS fits every 300 K.

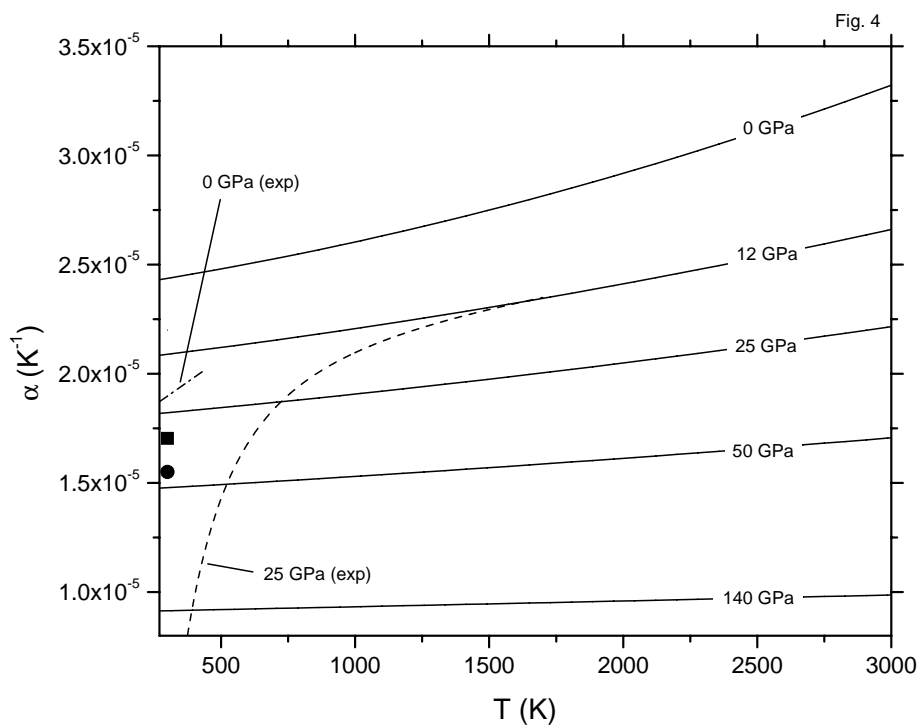


Figure 4. Volume coefficient of thermal expansion. Solid curves are from this work. Other symbols, from experimental work as follows: dashed curve (0 GPa), *Wang et al.* [1994]; circle (0 GPa), *Fiquet et al.* [1998]; square (0 GPa) and dashed-dotted line (25 GPa), *Funamori et al.* [1996]

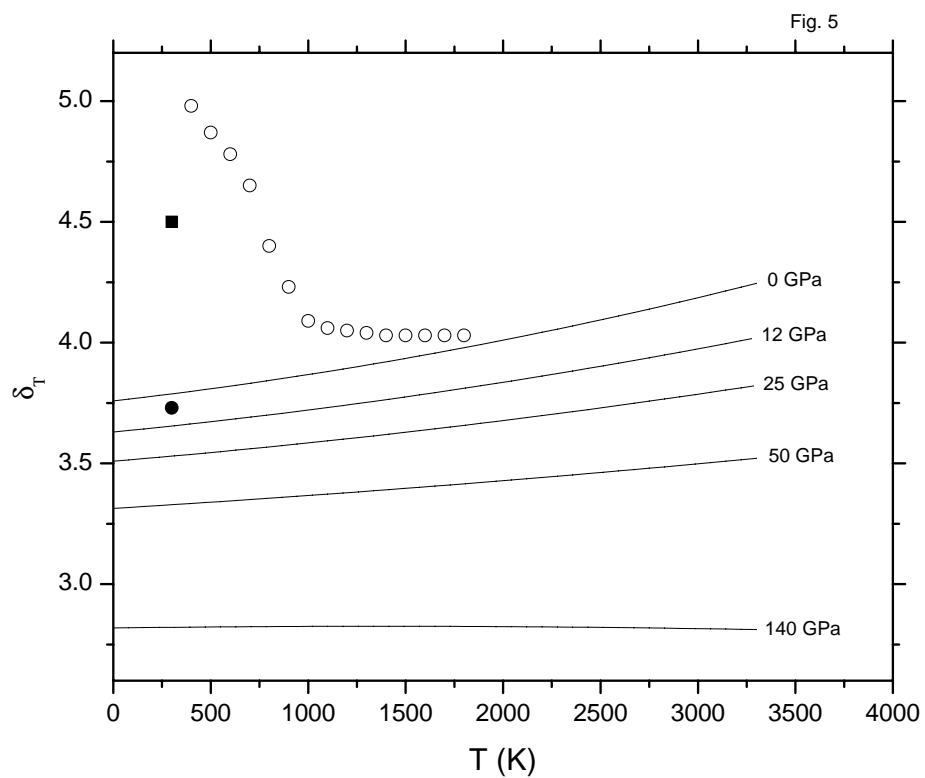


Figure 5. Anderson-Grüneisen parameter as a function of temperature. The circle is the experimentally determined value from *Wang et al.* [1994]. The square is the value determined by *Masuda and Anderson* [1995] from the experimental data of *Utsumi et al.* [1995]. Open circles are δ_T s determined from Debye theory by *Anderson* [1998].

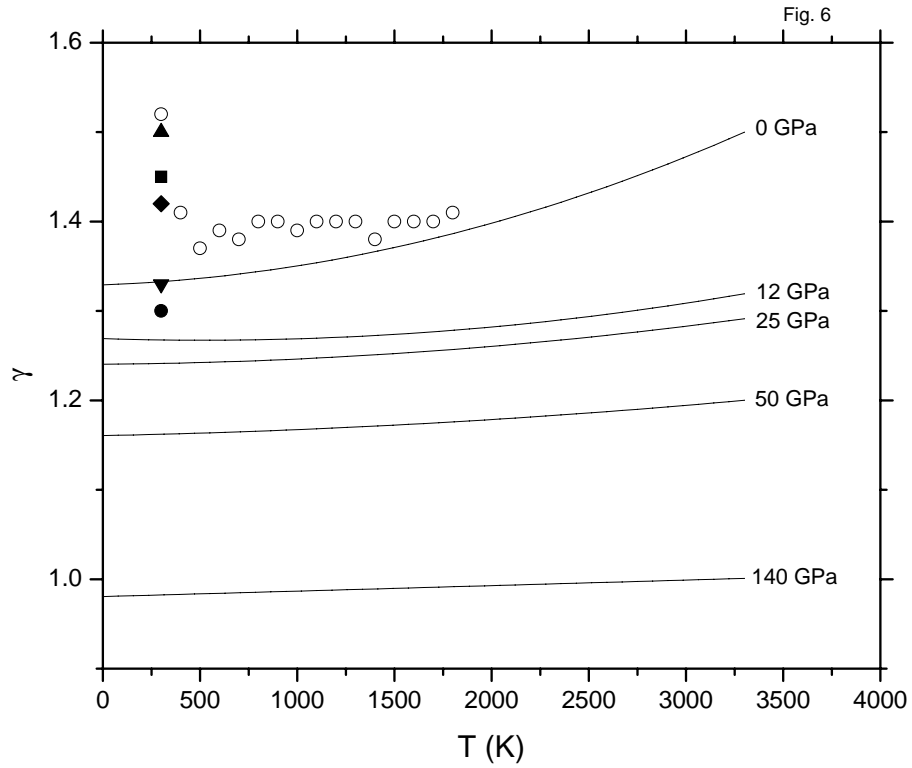


Figure 6. Grüneisen parameter as a function of temperature. The solid circle is the experimentally determined value from *Wang et al.* [1994], and the square is the value determined by *Masuda and Anderson* [1995] from the experimental data of *Utsumi et al.* [1995]. Other symbols are from inversion of multiple experimentally determined data sets: triangle, *Bina* [1995]; inverted triangle, *Jackson and Rigden* [1996]; and diamond, *Shim and Duffy* 2000]. Open circles are γ s determined from Debye theory by *Anderson* [1998].

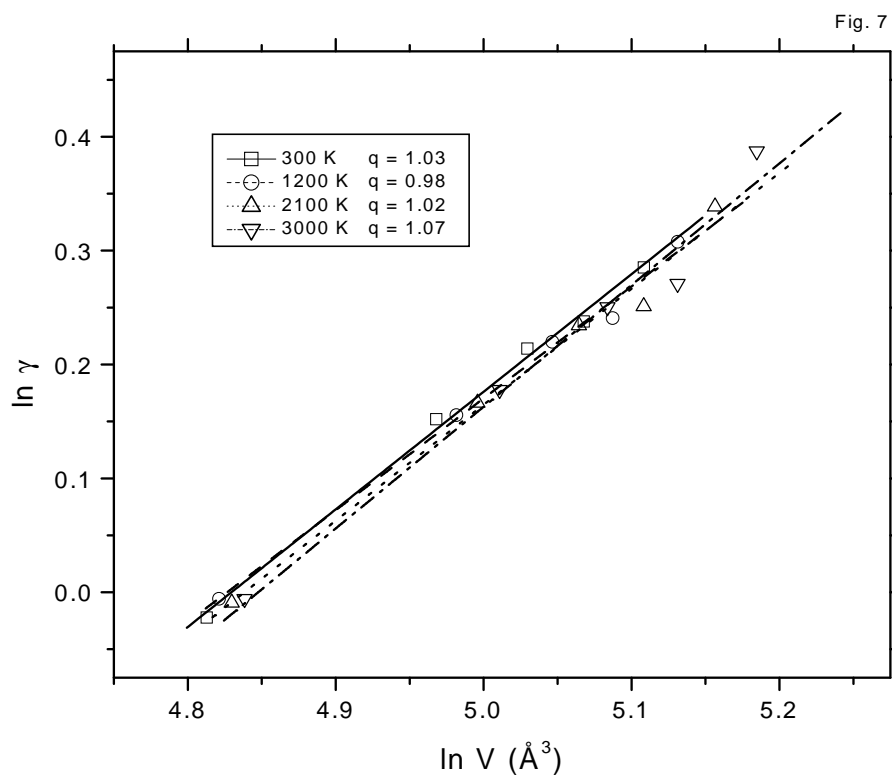


Figure 7. The $\ln \gamma$ versus $\ln V$. The slope of each curve gives q : solid curve and squares, 300 K; dashed curve and circles, 1200 K; dotted curve and triangles, 2100 K; dash-dotted curve and inverted triangles, 3000 K. The lower temperatures are all close to 1, with a slight rise to 1.07 at 3000 K.

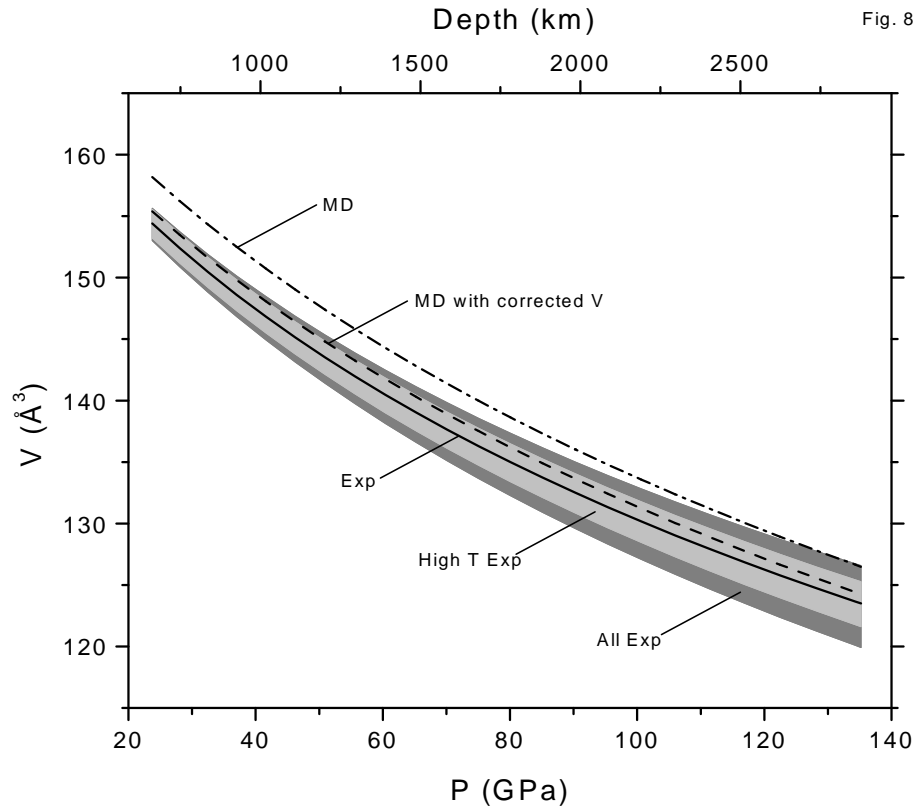


Figure 8. Volumes of MgSiO_3 perovskite along the geothermal gradient of *Brown and Shankland* [1981]. Dash-dotted curve is volume from our Universal EOS fit. Dashed curve is from our Universal fit with V_0 fixed to 162.49 \AA^3 [*Mao et al.*, 1991]. Dotted curve is for experimental data sets with V_0 fixed to 162.49 \AA^3 (see Table 2). Both high temperature (F98+F00+S99) and all MgSiO_3 data sets fall on the same line. Shaded areas indicate the uncertainties in the fits of the experimental data sets.

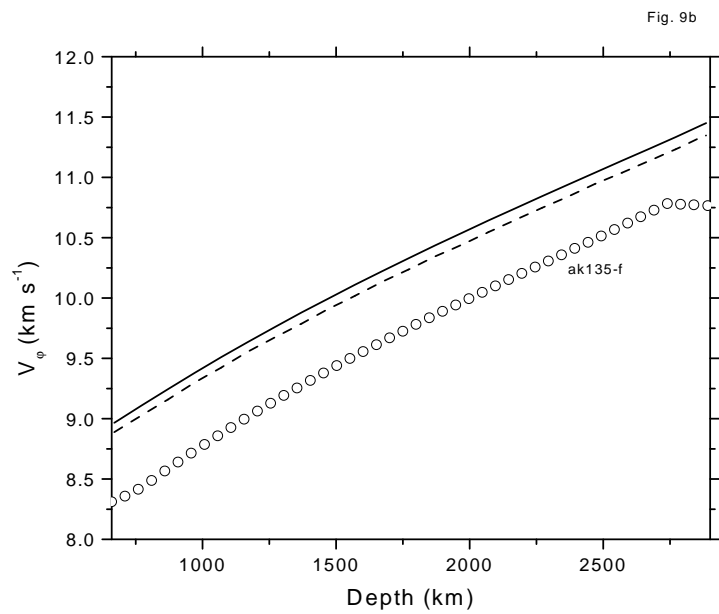
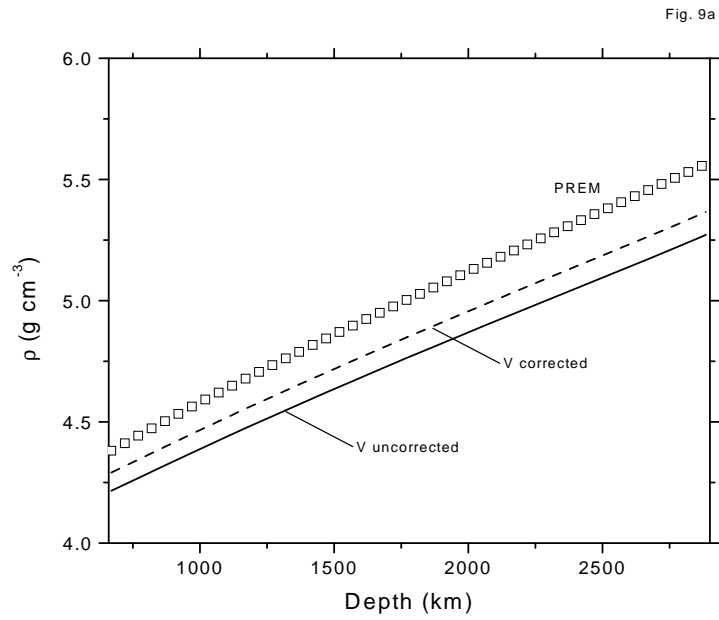


Figure 9. (a) Densities and (b) bulk sound velocities of MgSiO_3 perovskite calculated along the lower mantle geotherm of *Brown and Shankland* [1981] using the thermal Universal EOS. Solid curve is for uncorrected volumes and dashed curve is for V_0 set to the experimental value of *Mao et al.*, [1991]. Squares are densities from PREM [*Dziewonski and Anderson*, 1981]. Circles are velocities from the ak135-f seismological model [*Kennett et al.*, 1995; *Montagner and Kennett*, 1996].

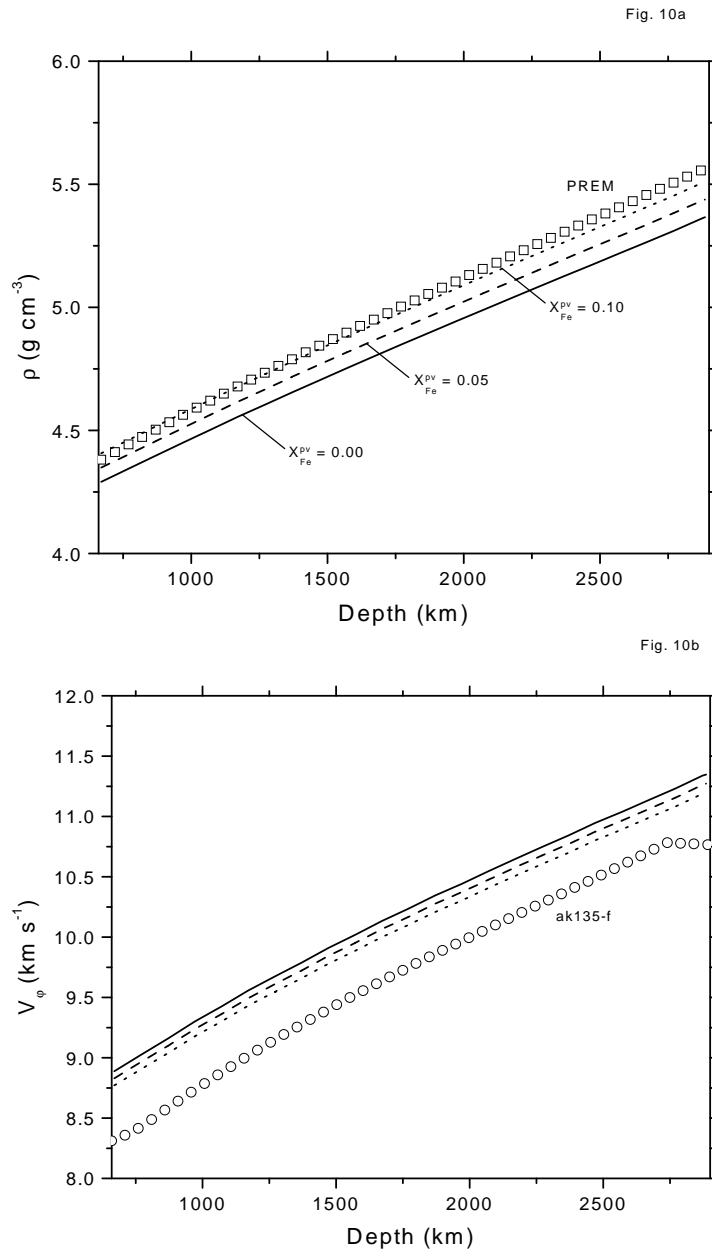


Figure 10. (a) Densities and (b) bulk sound velocities of $(\text{Mg,Fe})\text{SiO}_3$ perovskite calculated along the geotherm of *Brown and Shankland* [1981] using the experimental value of V_0 *Mao et al.*, [1991] for $X_{\text{Fe}}^{\text{pv}} = 0.00$ (solid curve), 0.05 (dashed curve), and 0.10 (dotted curve). Squares are densities from PREM [*Dziewonski and Anderson, 1981*]. Circles are velocities from the ak135-f seismological model [*Kennett et al., 1995; Montagner and Kennett, 1996*].

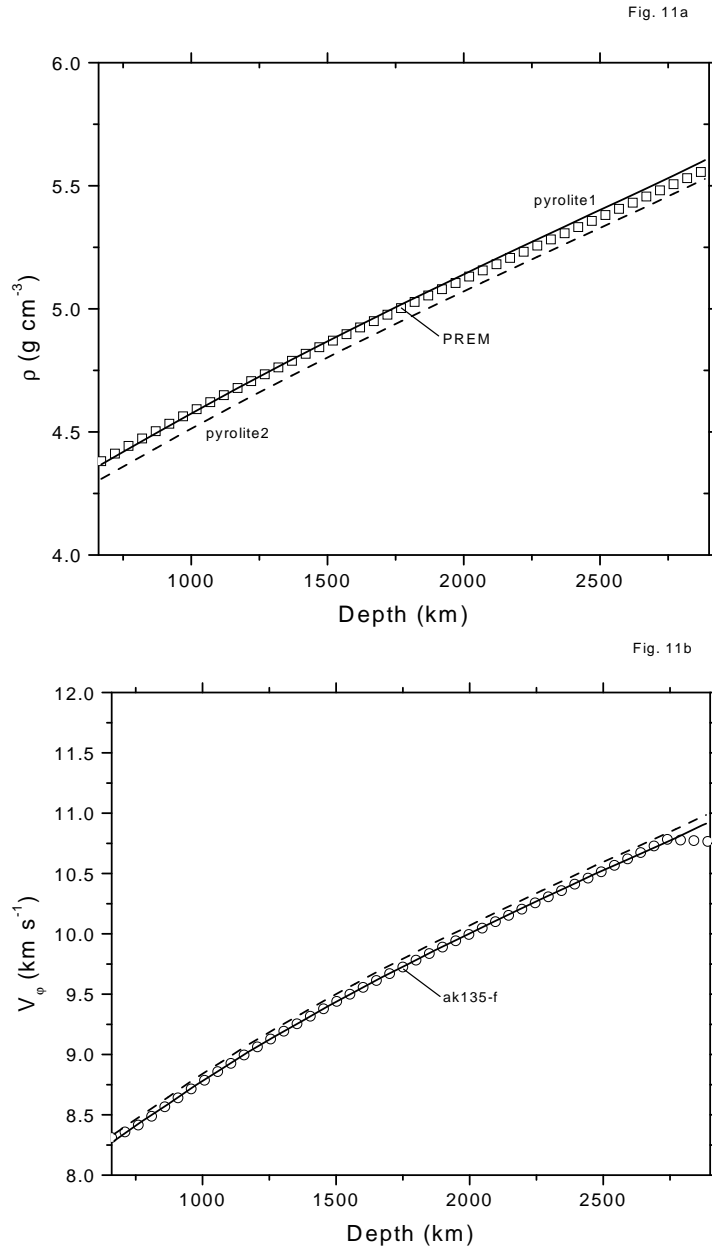


Figure 11. (a) Densities and (b) bulk sound velocities of two simplified pyrolite models (67 vol % pv, 33 vol % mw) along the geotherm of *Brown and Shankland* [1981]. Solid curve is $X_{\text{Mg}}^{\text{pv}} = 0.93$, $X_{\text{Mg}}^{\text{mw}} = 0.82$. Dashed curve is $X_{\text{Mg}}^{\text{pv}} = 0.96$, $X_{\text{Mg}}^{\text{mw}} = 0.86$. Squares are densities from PREM [*Dziewonski and Anderson, 1981*]. Circles are velocities from the ak135-f seismological model [*Kennett et al., 1995; Montagner and Kennett, 1996*].

Table 1. MD P-V-T Data Used in EOS Fits

P, GPa	T, K	a, Å	b, Å	c, Å	V, Å ³
0	300	4.8166	4.9283	6.9649	165.33
0	600	4.8299	4.9397	6.9787	166.50
0	900	4.8439	4.9519	6.9944	167.77
0	1200	4.8586	4.9648	7.0107	169.11
0	1500	4.8732	4.9769	7.0289	170.48
0	1800	4.8886	4.9901	7.0455	171.87
0	2100	4.9109	5.0145	7.0578	173.80
0	2400	4.9311	5.0354	7.0688	175.52
0	2700	4.9525	5.0538	7.0831	177.28
0	3000	4.9672	5.0633	7.1076	178.76
12	900	4.7790	4.8856	6.8895	160.86
12	1200	4.7917	4.8951	6.9024	161.90
12	1500	4.8036	4.9051	6.9165	162.97
12	1800	4.8169	4.9157	6.9288	164.06
12	2100	4.8295	4.9256	6.9441	165.18
12	2400	4.8429	4.9367	6.9586	166.36
12	2700	4.8628	4.9539	6.9690	167.88
12	3000	4.9035	4.9531	6.9695	169.27
25	300	4.6971	4.8093	6.7728	152.99
25	600	4.7073	4.8169	6.7830	153.80
25	900	4.7181	4.8250	6.7948	154.68
25	1200	4.7285	4.8330	6.8055	155.53
25	1500	4.7390	4.8409	6.8166	156.38
25	1800	4.7497	4.8487	6.8291	157.27
25	2100	4.7609	4.8572	6.8408	158.19
25	2400	4.7728	4.8658	6.8514	159.11
25	2700	4.7850	4.8736	6.8645	160.08
25	3000	4.8015	4.8859	6.8773	161.34
50	900	4.6194	4.7307	6.6445	145.20
50	1200	4.6280	4.7366	6.6531	145.84
50	1500	4.6366	4.7414	6.6632	146.48
50	1800	4.6450	4.7474	6.6726	147.14
50	2100	4.6545	4.7524	6.6821	147.81
50	2400	4.6627	4.7589	6.6920	148.49
50	2700	4.6728	4.7644	6.7014	149.20
50	3000	4.6814	4.7700	6.7129	149.90
140	300	4.3572	4.5023	6.2698	123.00
140	600	4.3627	4.5046	6.2768	123.35
140	900	4.3687	4.5076	6.2839	123.74
140	1200	4.3747	4.5097	6.2903	124.10
140	1500	4.3806	4.5121	6.2967	124.46
140	1800	4.3867	4.5146	6.3027	124.82
140	2100	4.3923	4.5164	6.3104	125.18
140	2400	4.3986	4.5186	6.3170	125.55

Table 1. (continued)

P, GPa	T, K	a, Å	b, Å	c, Å	V, Å ³
140	2700	4.4048	4.5209	6.3235	125.92
140	3000	4.4109	4.5230	6.3309	126.31

Table 2. Equation of State Parameters^a

	$V_0, \text{\AA}^3$	K_{T_0}, GPa	K'_{T_0}	a, GPa	$b, \text{GPa K}^{-1}$	χ^2, GPa
This work						
Birch-Murnaghan EOS	165.40(6)	274(1)	3.73(2)	-2.00(2)	0.00667(5)	0.08561
Universal EOS	165.40(5)	273(1)	3.86(2)	-1.99(1)	0.00664(5)	0.06712
Experimental results						
M91	162.49(7)	261(4)	4 ^b			
F98	162.65(15)	262(6)	3.41(22)	-1.79(21)	0.00597(70)	1.47438
	162.49 ^c	267(3)	3.25(10)	-1.79(21)	0.00597(70)	1.41566
	162.60(9)	264 ^d	3.33(2)	-1.79(21)	0.00596(69)	1.41333
	162.49 ^c	264 ^d	3.41(3)	-1.80(35)	0.00601(73)	1.36143
F00	162.74(56)	239(8)	4.41(18)	-1.85(6)	0.00618(20)	0.61052
	162.49 ^c	245(4)	4.29(11)	-1.85(6)	0.00618(20)	0.59369
	161.68(18)	264 ^d	3.88(2)	-1.85(6)	0.00617(20)	0.60570
	162.49 ^c	264 ^d	3.52(4)	-1.73(8)	0.00577(28)	1.23307
S99	163.25(63)	242(6)	4.45(10)	-1.72(1)	0.00574(2)	0.26719
	162.49 ^c	256(5)	4.20(10)	-1.72(1)	0.00572(2)	0.26227
	161.10(28)	264 ^d	4.06(4)	-1.71(1)	0.00572(2)	0.26645
	162.49 ^c	264 ^d	3.89(2)	-1.75(2)	0.00584(7)	0.31819
F98 + F00 + S99	162.93(33)	235(6)	4.72(13)	-1.85(12)	0.00618(38)	1.56307
	162.49 ^c	244(4)	4.52(13)	-1.86(12)	0.00621(40)	1.55478
	161.69(22)	264 ^d	4.08(1)	-1.87(12)	0.00622(38)	1.61901
	162.49 ^c	264 ^d	3.75(2)	-1.73(15)	0.00577(7)	2.22349
All	162.31(10)	249(6)	4.40(20)	-1.92(10)	0.00639(32)	0.60337
	162.49 ^c	243(8)	4.55(28)	-1.90(10)	0.00635(34)	0.61628
	162.01(22)	264 ^d	3.92(8)	-1.88(10)	0.00628(38)	0.67860
	162.49 ^c	264 ^d	3.75(2)	-1.67(20)	0.00557(65)	1.04352

^aMD are best fit EOS parameters to molecular dynamics P-V-T data. Experimental results are the best fit Universal EOS parameters to experimental data sets, except data taken from *Mao et al.* [1991] (M91). Remaining experimental results are F98, *Fiquet et al.* [1998] (27 data points); F00, *Fiquet et al.* [2000] (38 data points); S99, *Saxena et al.* [1999], (37 data points); All, all $X_{\text{Mg}} = 1.0$ data (363 data points; see Figure 1). Values in parentheses are standard deviations.

^bFixed equal to 4.

^cFixed to V_0 from *Mao et al.* [1991].

^dFixed to K_{T_0} from *Yeganeh-Haeri* [1994].

Table 3. Zero Temperature Equation of State Parameters

	V, Å ³	K, GPa	K'
This work ^a	164.22	280	3.84
PIB ^b	164.78	252	4.05
LAPW ^c	160.74	266	4.2
PWPP ^d	157.50	259	3.9

^aUniversal fit. Other theoretical fits are third-order Birch-Murnaghan fits.

^b*Cohen* [1987].

^c*Stixrude and Cohen* [1993].

^d*Wentzcovitch et al.* [1995].